

OPEN

Novel and selective inactivators of Triosephosphate isomerase with anti-trematode activity

Florencia Ferraro^{1,8}, Ileana Corvo^{1,8}, Lucia Bergalli², Andrea Illarraz¹, Mauricio Cabrera¹, Jorge Gil³, Brian M. Susuki⁴, Conor R. Caffrey⁴, David J. Timson⁵, Xavier Robert⁶, Christophe Guillon⁶, Teresa Freire⁷ & Guzmán Álvarez^{1*}

Trematode infections such as schistosomiasis and fascioliasis cause significant morbidity in an estimated 250 million people worldwide and the associated agricultural losses are estimated at more than US\$ 6 billion per year. Current chemotherapy is limited. Triosephosphate isomerase (TIM), an enzyme of the glycolytic pathway, has emerged as a useful drug target in many parasites, including *Fasciola hepatica* TIM (*FhTIM*). We identified 21 novel compounds that selectively inhibit this enzyme. Using microscale thermophoresis we explored the interaction between target and compounds and identified a potent interaction between the sulfonyl-1,2,4-thiadiazole (compound 187) and *FhTIM*, which showed an IC_{50} of 5 μ M and a K_d of 66 nM. In only 4 hours, this compound killed the juvenile form of *F. hepatica* with an IC_{50} of 3 μ M, better than the reference drug triclabendazole (TCZ). Interestingly, we discovered *in vitro* inhibition of *FhTIM* by TCZ, with an IC_{50} of 7 μ M suggesting a previously uncharacterized role of *FhTIM* in the mechanism of action of this drug. Compound 187 was also active against various developmental stages of *Schistosoma mansoni*. The low toxicity *in vitro* in different cell types and lack of acute toxicity in mice was demonstrated for this compound, as was demonstrated the efficacy of 187 *in vivo* in *F. hepatica* infected mice. Finally, we obtained the first crystal structure of *FhTIM* at 1.9 Å resolution which allows us using docking to suggest a mechanism of interaction between compound 187 and TIM. In conclusion, we describe a promising drug candidate to control neglected trematode infections in human and animal health.

Trematode infections are a major cause of human disability and mortality in many developing countries, and remain one of the most important challenges for medicine in the 21st century^{1–3}. An estimated 250 million people worldwide suffer these infections. Moreover, the *Fasciola* and *Schistosoma* parasites infect cattle, sheep and other animals of agricultural importance with estimated agricultural losses of more than US\$ 6 billion per year⁴. In spite of their morbidity and economic impact, neither disease is of sufficient pharmaceutical industry interest for the development of new drugs, such that anthelmintic therapy relies precariously on just two drugs that were developed over 40 years ago: triclabendazole (TCZ) for fascioliasis and praziquantel (PZQ) for schistosomiasis^{1,2}. The over-reliance on TCZ to treat sheep and, to a lesser extent, cattle, has resulted in selection for flukes resistant to TCZ. For PZQ, although clinically-relevant resistance has yet to emerge, resistance has been reported on occasion in the field and in various experimental settings^{5–7}.

An important characteristic in the metabolism of trematode parasites is their dependence on glycolysis as an energy source for survival⁸. Thus, enzymes in the glycolytic pathway are attractive targets in the search for

¹Laboratorio de Moléculas Bioactivas, Universidad de la República, CENUR Litoral Norte, Paysandú, Uruguay.

²Departamento de Química del Litoral, Universidad de la República, CENUR Litoral Norte, Paysandú, Uruguay.

³Laboratorio de Reproducción Animal, Producción y Reproducción de Rumiantes, CENUR Litoral Norte-Facultad de Veterinaria, Universidad de la República, Paysandú, Uruguay. ⁴Center for Discovery and Innovation in Parasitic Diseases, Skaggs School of Pharmacy and Pharmaceutical Sciences, University of California San Diego, La Jolla, CA, USA. ⁵School of Pharmacy and Biomolecular Sciences, The University of Brighton, Brighton, UK.

⁶Equipe Rétrovirus et Biochimie Structurale, Université de Lyon, CNRS, MMSB, Lyon, France. ⁷Laboratorio de Inmunomodulación y Desarrollo de Vacunas, Departamento de Inmunobiología, Facultad de Medicina, Universidad de República, Montevideo, Uruguay. ⁸These authors contributed equally: Florencia Ferraro and Ileana Corvo. *email: guzmanalvarezlq@gmail.com

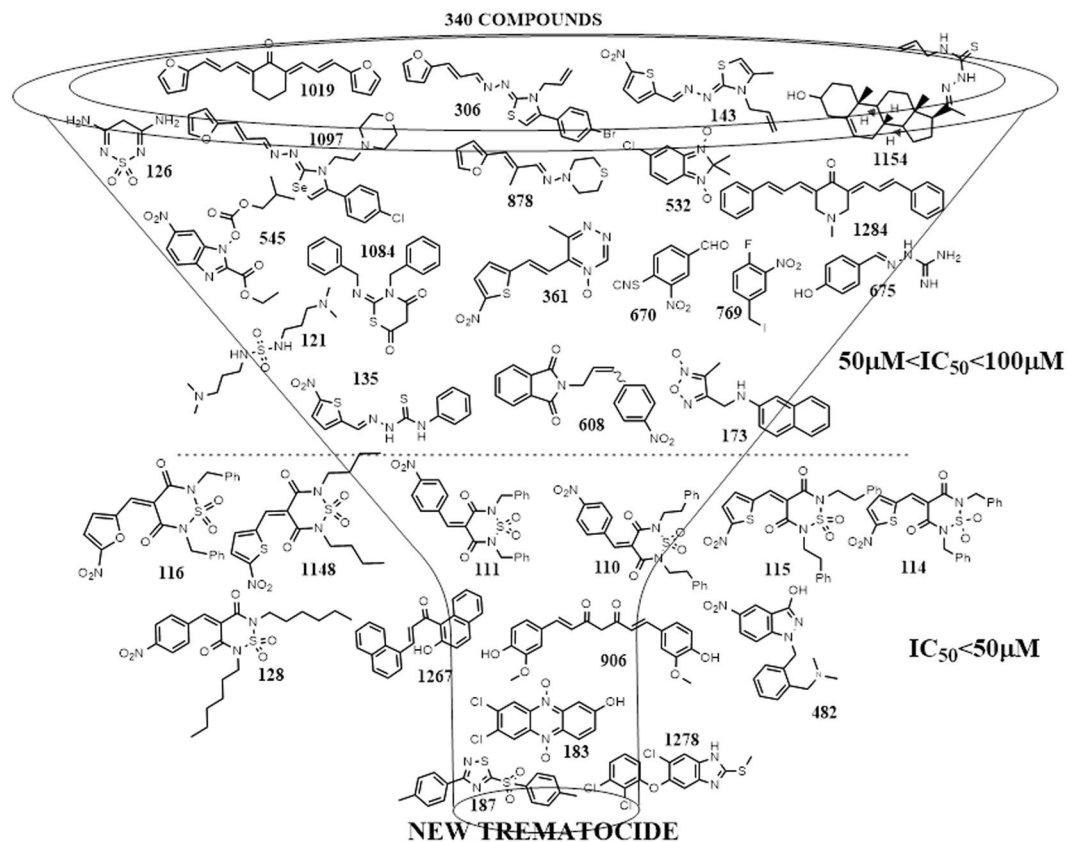


Figure 1. Inhibition cascade for a screen of 340 small molecules with recombinant *FhTIM*. Structures of the best inhibitors are shown. Compounds are numbered according to Supplementary Table 1S. Three ranges of inhibitory activity were established: $\text{IC}_{50} > 100 \mu\text{M}$ (no activity, not shown), IC_{50} values between 50 and $100 \mu\text{M}$ (moderate activity) and $\text{IC}_{50} < 50 \mu\text{M}$ (good activity).

new small molecules chemotherapies^{9,10}. One enzyme, triosephosphate isomerase (TIM; EC 5.3.1.1), is of particular interest as an anthelmintic target⁸. TIM catalyzes the isomerization of glyceraldehyde-3-phosphate and dihydroxyacetone phosphate in the fifth step of the glycolytic pathway¹¹. It also has moonlighting functions, as it is found differently expressed in many types of cancer, it participates in the regulation of the cell cycle, function as an auto-antigen and in the evasion of the immune response, as a virulence factor in some organisms¹². Structurally, most of the known TIMs are homodimers, each monomer consisting of eight parallel β -strands surrounded by eight α -helices that, together, form a typical “TIM barrel” fold. The interface between monomers occupies a significant portion of the molecular surface area of each monomer, approximately 1500 \AA^2 ^{13–15}. Because TIM is active only in its dimeric form, small molecules that engage the interface may interfere with proper enzyme function¹⁶.

Encouraged by the fact that only 50% of the residues involved in the dimer interface are conserved between trematode TIMs and their human ortholog¹⁷, we aimed to identify molecules that specifically engage the parasite TIM interface. Accordingly, using 340 *in-house* compounds, we screened *in vitro* recombinant *FhTIM* for low micromolar inactivators. With the best compounds, we performed selectivity assays (using mammalian TIMs) and preclinical studies (toxicology in mammalian cells and in mice). We evaluated their efficacy *in vivo* in mice infected with *F. hepatica* and perform X-Ray and docking studies to elucidate the mechanism of inhibition.

Results

Screening *FhTIM*. We hypothesized that a TIM dimer interface inactivator would be a successful strategy to identify molecules with selective antiparasitic activity^{18–20}. Therefore, we selected 340 compounds from our *in-house* chemical collection and screened them against the isolated recombinant *FhTIM*. In this work, the screened chemotypes are represented in Fig. 1 (benzofuroxanes, furanes and thiophenes, 4-substituted-1,2,6-thiadiazines, quinoxaline 1,4-dioxides, phenazine 5,9-dioxides, furoxanes, imidazole *N*-oxides, indazoles and others). Around 10% of the evaluated compounds were active with an $\text{IC}_{50} < 100 \mu\text{M}$ (concentration leading to at least 50% inhibition). Most of the families possess at least one active compound, except for the twenty evaluated quinoxalines from which no active molecules were found. Those families with a high percentage of active derivatives were the 4-substituted-1,2,6-thiadiazines, selenocompounds and phenazines, 60% (9/15), 100% (3/3) and 67% (2/3) active, respectively. We found 30–40% of inactivators among the thiadiazines and their precursors, and the curcuminoids family (Supplementary Table 1S). We established an $\text{IC}_{50} < 50 \mu\text{M}$ as the cut-off for good activity (Table 1). Only one active compound belongs to the thiaziazole chemotype (compound 187, Fig. 1), which had

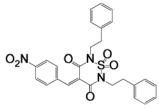
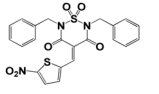
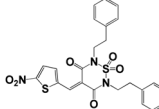
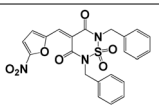
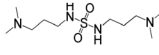
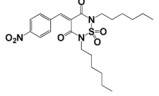
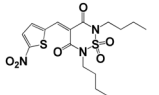
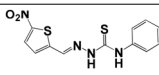
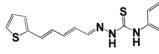
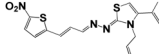
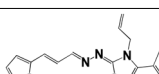
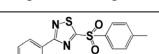
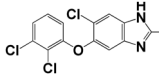
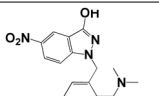
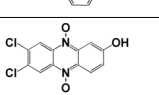
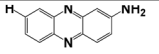
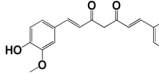
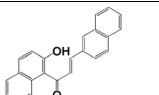
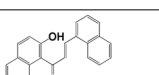
Compound identifier	Structure	IC ₅₀ (μM)	K _d (μM)
110		7 ± 1	nd*
114		25 ± 8	664 ± 25
115		8 ± 2	120 ± 12
116		5 ± 1	nd
121		50 ± 9	nd
128		5 ± 1	120 ± 10
1148		15 ± 5	nd
135		50 ± 8	nd
310		79 ± 7	nd
144		60 ± 2	nd
1134		45 ± 4	nd
187		4.0 ± 0.2	0.07 ± 0.01
1278 (TCZ)		7 ± 1	1000
482		30 ± 3	nd
183		25 ± 3	nd
1149		50 ± 6	nd
906		35 ± 4	nd
1254		50 ± 5	nd
1267		35 ± 2	nd

Table 1. IC₅₀ values of the best TIM inactivators and experimental K_d values by MST. *nd. not determined.

Compound	<i>F. hepatica</i>		<i>S. mansoni</i> somules severity score*	Toxicity mammalian cells**
	IC ₅₀ (μ M)	incubation time (h)		
906	7 \pm 1	4	nd***	T
110	5 \pm 2	30	0	T
114	6.5 \pm 0.6	4	4 (72 h)	T
115	7 \pm 2	72	4 (72 h)	T
116	>50	72	Nd	nd
128	10 \pm 1	12	Nd	T
1148	12 \pm 2	4	0	nd
144	25 \pm 5	72	4 (72 h)	NT
1134	50 \pm 6	72	Nd	NT
187	3.0 \pm 0.5	4	4 (24h)**	NT
1293 [†]	50	48	Nd	nd
1278 (TCZ)	>50	72	Nd	NT

Table 2. The activity of the best compounds against juvenile forms of *F. hepatica* and *S. mansoni* somules. *Severity score defined in Methods (*S. mansoni*: treatment of somules *in vitro* and adults *ex vivo*). **The selectivity index for the effect on the parasite vs. mammalian cells, NT represents an SI >10 when the toxicity was <50% at 100 μ M vs. mammalian cells; ***nd, not determined; [†]sulfonyl derivative of the TCZ active metabolite [‡]Supporting video.

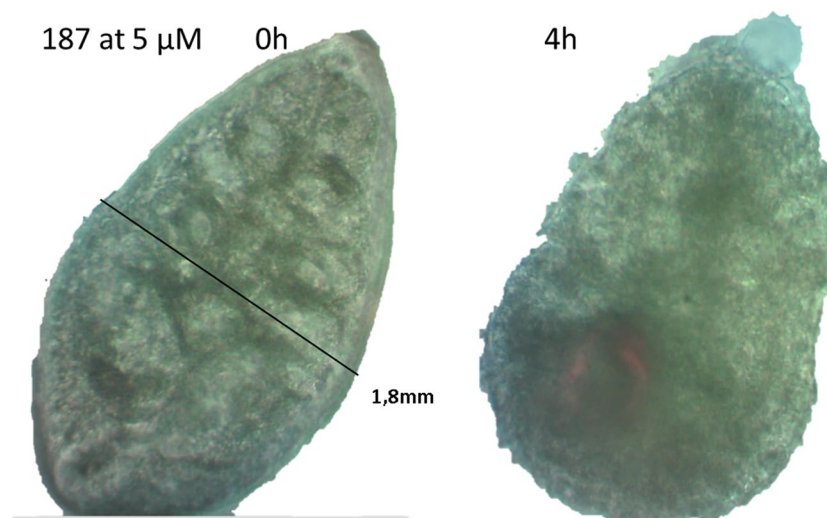


Figure 2. Optical microscopy (40 \times) photo of an NEJ from *F. hepatica* treated with compound **187** at 5 μ M at 0 and 4 hours of incubation (supporting video).

the greatest inhibition of the molecular target (Table 1). Interestingly, **TCZ** (compound **1278** in the collection) inhibited *FhTIM* with an IC₅₀ of 7 μ M (Table 1). In parallel, we performed MicroScale Thermophoresis (MST) with five representative molecules to evaluate their binding affinity. Among them, compound **187** showed the highest affinity for *FhTIM* with the lowest IC₅₀ (4.0 \pm 0.2).

Then we performed an *in vitro* selectivity assay of *FhTIM* as compared to human (*HsTIM*) and rabbit TIM as a representative ruminant animal²¹. The best *FhTIM* inhibitors, **110**, **115**, **128**, **187** and **TCZ**, were inactive (<20% inhibition) against *HsTIM* and rabbit TIM at 100 μ M.

In vitro and in vivo anti-parasite activity of the compounds. As a proof of concept, we tested the best *FhTIM* inactivators against *F. hepatica* and *S. mansoni* parasites. Also, we use compound **191** as a non-inhibitor which has a closely related structure to that of compound **187**. Some compounds were able to kill 100% of the newly excysted juvenile (NEJ) *F. hepatica* within 4 to 48 h (Table 2 and Fig. 2). Also, some of the compounds that were active against NEJ markedly affected *S. mansoni*, notably compound **187**, which, in the first 24 h, was lethal to somules, and decreased the motility of adults and the ability of their oral and ventral suckers to adhere to the floor of the culture dish well (Tables 2 and S2). In parallel, these compounds were assayed to characterize their non-specific toxicity against murine macrophages and bovine sperm. Both models are recommended by FDA as an *in vitro* prediction of toxicology²². We used fixed doses of 25 and 100 μ M of compound to test against the

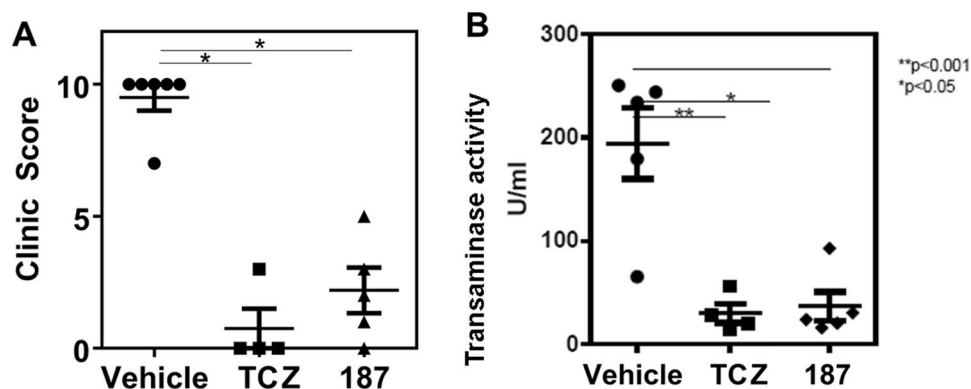


Figure 3. (A) Treatment of infected mice with one dose (100 mg/kg) of **187**, **TCZ** and as a control a lipidic emulsion (vehicle), (* $p < 0.05$). The “Clinic Score” is detailed in the methods section. (B) Transaminase profile at the end of the experiment.

mammalian cells: when the IC_{50} vs. the parasite was at least 10 times less than the IC_{50} vs. the mammalian cells, we considered these compounds as non-toxic (NT); if not, they were classified as toxic (T) (Table 2).

Then we tested the biological activity of compound **187** against the adult form of *F. hepatica* and *S. mansoni*. This compound was selected as it was the most potent and least toxic of our compounds and is active against the juvenile stages of *F. hepatica*. In the case of *F. hepatica*, parasites were affected in the first 4 h at 10 μ M (Fig. 2), ultimately leading to the death of all the parasites after 24 h. The *S. mansoni* parasite was also susceptible to compound **187**, showing decreased motility and loss of their ventral sucker adherence to the plate floor after 24 h at only 5 μ M.

Furthermore, the ability/potency of compound **187** to protect animals from *F. hepatica* infection was evaluated. To this end, BALB/c mice were infected with 10 *F. hepatica* metacercariae and one week later, compound **187** or **TCZ** were inoculated orogastrically. Compound **187**, together with **TCZ**, protected mice from the infection since they presented less severe clinical signs, including a decrease in liver necrosis, hemorrhage and splenomegaly (Fig. 3A). Then the transaminase profile was according to a healthy liver (Fig. 3B).

Finally, to get toxicological information about compound **187**, we performed acute oral toxicology (up-and-down experiment), which demonstrated an LD_{50} of ≥ 2000 mg/kg body weight in mice. An *in silico* exploration of the pharmacokinetic properties of compound **187** compared to the drug-likeness of other drugs gave parameters similar to those of the reference drug **TCZ** (Supplementary Fig. 2S).

Crystal structure of *Fh*TIM and prediction of compounds binding sites. To elucidate the molecular basis of *Fh*TIM inhibition, we obtained the crystal structure of *Fh*TIM at 1.9 Å resolution. The asymmetric unit displays three *Fh*TIM dimers (Fig. 4A). Each protomer shows a typical $(\beta/\alpha)_8$ TIM-barrel fold. The R.M.S.D. between *Fh*TIM and human TIM (*Hs*TIM, PDB ID: 4POC)²³ protomers is 4.5 Å on all $C\alpha$ pairs, in spite of only a 68% sequence homology. The catalytic pocket of each protomer in the *Fh*TIM structure is occupied by a sulfate molecule (SO_4^{2-}), likely from the crystallization buffer. The β/α loop 6 (residues 168–180 of *Fh*TIM) is known to open and close when accommodating the substrate in triosephosphate isomerases. Here, the loops are in the close conformation in all of the protomers of *Fh*TIM (Fig. 4B). Interestingly, the SO_4^{2-} ion is located in the same position as the phosphate group of the substrates (glyceraldehyde 3 P) in the *P. falciparum* (*Pf*TIM) or *S. aureus* TIM structures (PDB ID: 1LYX¹⁵ and 3UWU²⁴, respectively) through similar interactions (Fig. 4C). Indeed, the three unbound oxygen atoms of the O_4 tetrahedron in the triose phosphate moiety of *Pf*TIM interact with the main chain nitrogen of residues G175, S211, G236 and G237, as do 3 out of 4 oxygen atoms of the *Fh*TIM SO_4^{2-} . The remaining oxygen of the SO_4^{2-} present in the *Fh*TIM structure (and spatially corresponding to the oxygen atom linking the phosphate to the sugar in the natural substrate) is coordinated by a water molecule roughly located at the position of the distal carbon of the substrate analog in *Pf*TIM (Fig. 4C). This suggests that the O_4 tetrahedron drives the orientation of the substrate in the catalytic pocket.

Attempts to understand the mechanism of interaction between the inhibitors and TIM via crystallization did not yield ligand-bound structures. Thus, we used the crystal structure obtained for *Fh*TIM to perform docking studies with our compounds. For each compound, we performed 10 docking calculations including the 10 best poses, *i.e.*, 100 positions selected per compound, which were then clustered and ranked. For each compound, the 10 best positions out of these resulting datasets are included in the supporting material. Docking was performed using four different strategies: “blind” docking on the whole surface of *Fh*TIM in the dimeric and the monomeric form, as well as targeted docking of only the active site with and without the flexibility of the residues in the active site pocket.

No preferential binding sites of the compounds could be identified on the surface of the dimer (Supplementary Material Fig. 1S). However, on the surface of the monomer, the compounds with the best IC_{50} in Table 1, including the anti-*F. hepatica* drug, **TCZ**, bind mostly to one region, which is directly involved in the dimerization (Fig. 5 and Supplementary Material Fig. 1S) with predicted affinities in the micromolar range. Given the size of the dimeric interface, these affinities would probably not be sufficient to disrupt a pre-formed dimer but the compounds might impair the dimerization of monomers or result in a modification of the dimer conformation. Noteworthy, compounds docked on the dimeric interface are predicted to bind close to crucial residues for TIM

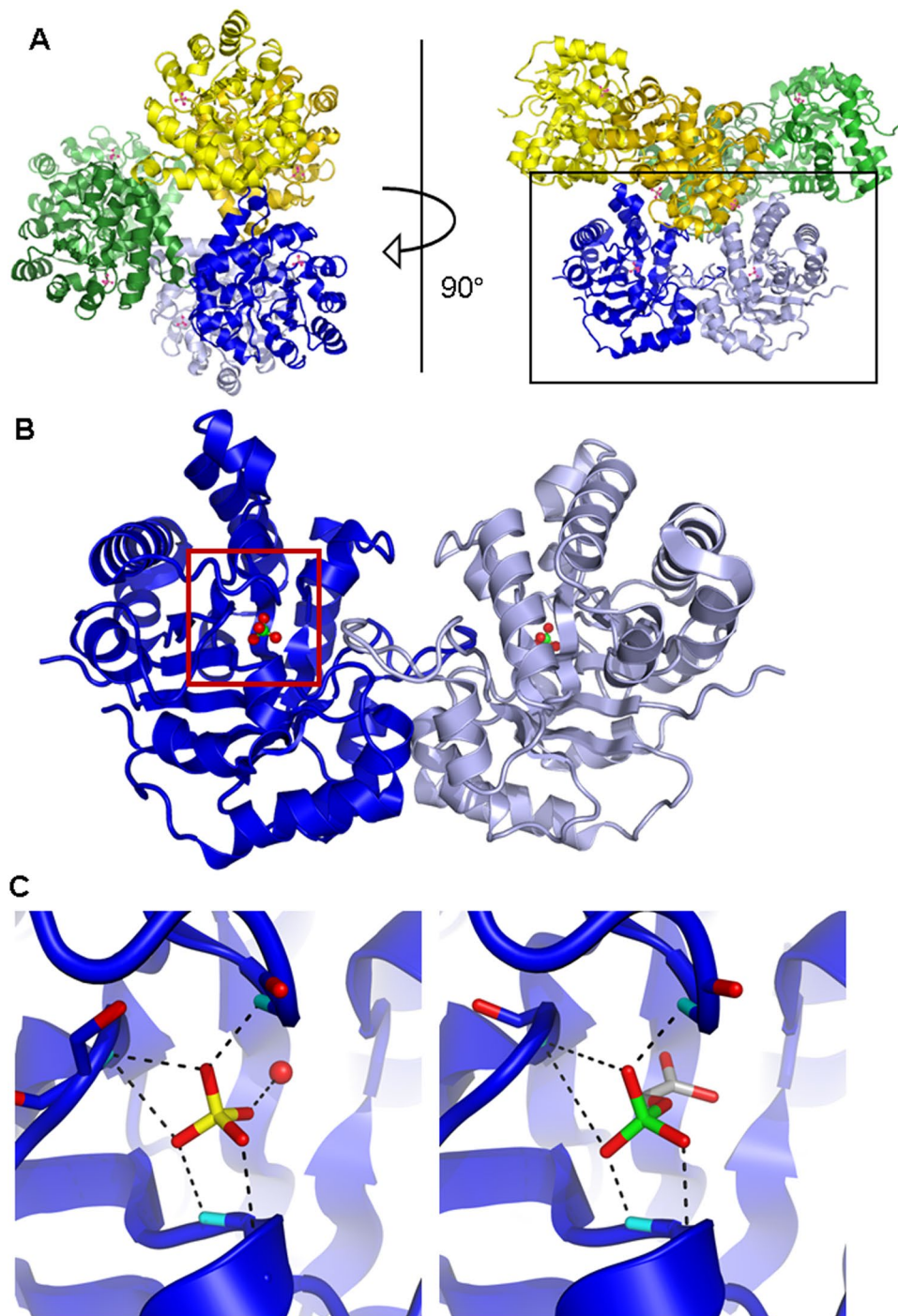


Figure 4. (A) Top (left) and side (right) view of the content of the asymmetric unit of *FhTIM* crystal. Dimer A-D: blue tints; dimer B-C: green tints; dimer E-F: yellow tints, with one SO_4^{2-} molecule (green and yellow) per protomer. Black rectangle highlights the dimer shown in B; (B) Close-up view of dimer A-D with the two SO_4^{2-} molecules in the active site of each monomer (red and green). Red rectangle highlights the active site of *FhTIM* shown in (C), left panel; (C) Close-up comparison of the active site of chain A of *FhTIM* (left panel) with the active site of chain A of *PfTIM* (PDB ID: 1LYX, right panel) with their liganded SO_4^{2-} and phosphoglycolate (PGA), respectively. Dashed lines display the hydrogen bonds network of the ligand with neighboring residues/water molecules. The red sphere in the left panel corresponds to water molecule 465 of *FhTIM*, chain A. Coloring scheme for the ligands' atoms is: red = oxygen, yellow = phosphorus, green = sulfur, light gray = carbon, orange = chloride. The structure of *FhTIM* is available in the PDB database (accession ID: 6R8H).

function. Indeed, the three representative compounds (**1278**, **110** and **187**) are located in close contact of K14 (less than 4 Å), and of these, **187** and **1278** (TCZ) are also predicted to interact with residue H96 (Fig. 5C,E,G). Both K14 and H96 are directly involved in the interaction of TIM with its natural substrate. Thus, the compounds,

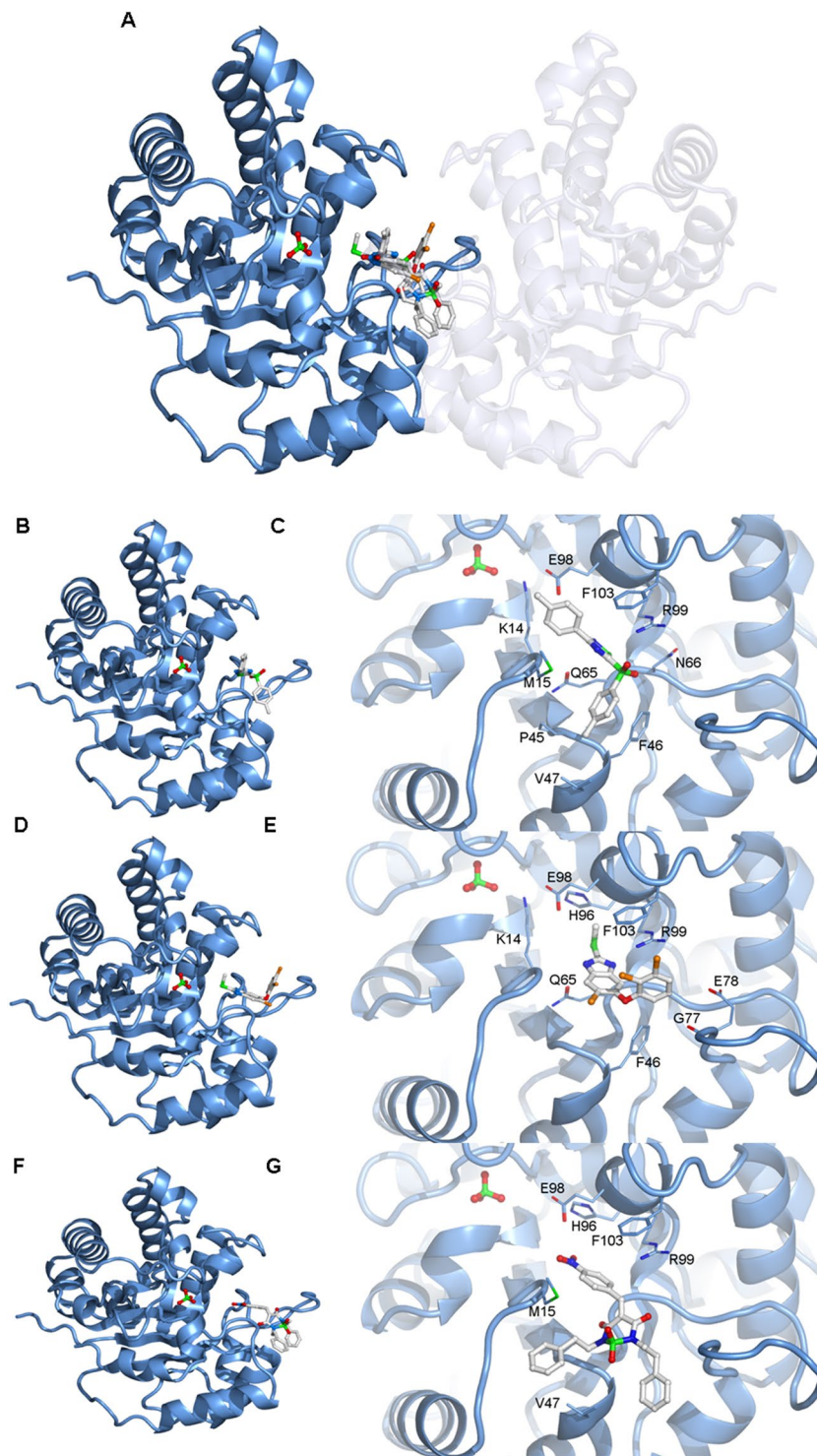


Figure 5. (A) Display of the best solutions for each compound after docking with compounds **110**, **187** and **TCZ** on the monomeric form of *FhTIM*. The position of the second monomer in the dimer is displayed as a ghost to show the location of the docked compounds compared to the dimeric interface. Best solution after docking of compounds **110** (B,C), **187** (D,E) and **TCZ** (F,G) on the *FhTIM* monomer. (B,D,F): Overall view of the position of the compounds. (C,E,G): close-up views of the position of the compounds with a display of the neighboring residues for which at least one atom lies within 4 Å of the ligand. These views are rotated 90° around the y-axis compared to panels B, D and F for the sake of clarity. The ligand coloring scheme is similar to Fig. 4C.

although not predicted to bind the active site, could inhibit interaction of TIM with its substrate. Anyhow, the docking experiments place the inactivators on a location of the dimer where they could have several effects on TIM function, which now need to be confirmed experimentally.

Discussion

We discovered eleven small molecules belonging to four chemical classes (curcuminoids, thiadiazines, thiosemicarbazides and sulfones) that inhibit recombinant *Fh*TIM. This is the first report of inactivators on this enzyme. Interestingly, we found that **TCZ**, the reference drug in the treatment of fasciolosis, inhibits *Fh*TIM. **TCZ**'s mechanism of action is still debated. It has been suggested that **TCZ** destabilizes β -tubulin²⁵, however, the direct evidence for interaction has not been demonstrated and the mechanism by which the parasites develop **TCZ** resistance does not appear to be the mutation of tubulin genes^{25,26}. The hypothesis that **TCZ** interacts with tubulin is based on the better-known mode of action of other benzimidazoles for which tubulin interaction has been demonstrated in antiparasitic and anticancer applications²⁷. The evidence for **TCZ**/tubulin interaction is weak and the structure of **TCZ**, in any case, is different from other anti-parasitic benzimidazoles²⁸. Our findings open the possibility of exploring TIM as a biological target of this drug.

Solving the first crystal structure of *Fh*TIM provided insights both on the enzyme's binding to natural substrates in the active site and the specific mechanism of action of our inactivators. Concerning the binding of substrate, the presence of a sulfate ion in the active site, and the fact that is orientated and coordinated as is the phosphate moiety of the substrate analog in *Pf*TIM¹¹, suggests that the O₄ tetrahedron is important for the correct orientation and coordination of the TIM substrate. Moreover, our finding of similar interactions between the SO₄²⁻ and the phosphate moieties of the natural substrate in the active site could explain why sulfate ions inhibited *Trypanosoma* TIM^{13,29} *in vitro* and may facilitate orienting drug-design efforts focused on sulfated/phosphorylated molecules.

Docking suggests that the efficient *Fh*TIM inactivators (**187**, **110**, **116**, **128**), including **TCZ**, bind tightly at the enzyme's dimerization interface (Fig. 5). As this dimerization is necessary for TIM function, our data suggest that our compounds could inhibit TIM by modifying or blocking the interface of the dimer. Inhibitors of protein:protein interactions have been sought for more than thirty years¹⁹ and although our compounds are small compared to the TIM interface, previous examples of small molecules inhibiting protein assembly have been described³⁰. Moreover, in our case, as the catalytic site is at the dimeric interface, a disturbance of the topology of the interface, even if not leading to the disassembly of the dimer, could be sufficient to inhibit TIM function. Also, we describe using dynamic studies for *T. cruzi* TIM a particular movement in solution in the same region that allows strong interactions in small molecules like **187**³¹. Then, a conformational change near the active site, could affect the correct substrate interaction in the active site. In particular, according to our docking results, the region of the dimeric interface putatively targeted by **TCZ** and our compounds are also close to residues K14 and H96, which are directly involved in the interaction of TIM with its natural substrate. Thus, **187** and **TCZ** may inhibit the binding of TIM to its substrate by blocking the catalytic loop in the closed, unfavorable conformation. Given the vicinity of the two zones, one cannot exclude that these two effects are involved in the inhibition by compounds **187** and **TCZ**. Such a dual effect would be very interesting from a pharmaceutical point of view, as the parasites would need to accumulate mutations against these two effects in order to become resistant to the treatment. Our docking data are *in silico* predictions, but they warrant further experiments to seek for a functional confirmation of the molecular mechanisms of inhibition by compounds **187** and **TCZ**.

The best *Fh*TIM inactivators are lethal to both juvenile and adult forms of *F. hepatica*, essentially immobilizing both developmental forms at 10 μ M after 4 h, a significant improvement over the activity of **TCZ** against both forms (the effect of **TCZ** was at 48 h at more than 50 μ M). Because TIMs are conserved proteins, including among trematodes^{8,31}, we demonstrated that the best *Fh*TIM inactivator compounds were also active against somules and adults of the *S. mansoni* bloodfluke. Of these, **144**, **1134** and **187**, were non-toxic to mammalian cells both herein, and previously at 100 μ M against murine macrophages and human peripheral blood mononuclear cells³². They were also more active against both parasites than the reference drug **TCZ** and its active metabolite **1293** (6-chloro-5-(2,3-dichlorophenoxy)-2-(methylsulfonyl)-1*H*-benzo[d]imidazole). The biological activity of **187** was observed immediately and developed faster than the other compounds. By contrast, it took several hours for **TCZ** to kill *Fasciola* NEJ *in vitro*. In addition, **187** displayed low toxicity in the acute oral toxicity assay. Moreover, its pharmacokinetic profile is comparable with commercially available drugs. This compound is also a moderate inhibitor of thioredoxin glutathione reductase (an essential core enzyme for redox homeostasis in flatworm parasites) and showed effect on NEJ and *Echinococcus granulosus* protoscolex at 48 h and a fixed dose of 20 μ M³². Also compound **187** protect mice infected with *F. hepatica* like the reference drug. We identified compound **187** as a lead candidate and obtained *Fh*TIM structure at 1.9 Å resolution crystals to understand the compound's ligand-binding characteristics. Compound **187** is the first, selective, anthelmintic TIM inactivator reported with *in vivo* efficacy. Altogether, our findings suggest that compound **187** is a good drug candidate for the treatment of flatworm infections. As these zoonotic parasites affect human and animal health, our compound **187** seems a good lead to developing a new class of "all-in-one" drugs with broad anti-parasitic potential.

Methods

Chemicals. The studied compounds were selected from our chemo library (LIDENSA) using the following criteria: (i) agents belonging to *T. cruzi* TIM inhibitors, or/and (ii) symmetrical and benzo-containing agents, structurally related to previously described TIM inhibitors. The selected compounds belong to fourteen chemotypes: 1-thiazoles, 2-thiadiazoles, 3-quinoxalines, 4-thiosemicarbazides, 5-steroids, 6-thiadiazines and precursors, 7-selenocompounds, 8-hydrazines, 9-curcuminoids, 10-indazoles, 11-imidazoles, 12-benzo-furoxanes, 13-triazines, 14-phenazine and 40 molecules with diverse structures not clustered in any family. The purity of the compound was checked only with the active molecules, reaching more than 98% by HPLC-MS. The synthetic procedures for the selected active compounds were described previously compound **187**³³, thiadiazine compounds³⁴, compound **482**³⁵. Compound **1278** is **TCZ**, which is a commercially available anti-fascioliasis drug (batch PS059349, 98.9% pure from Andres Pinaluba S.A.)

Microscale thermophoresis. MST experiments were performed according to the NanoTemper technologies protocol in a Monolith NT.115 (red/blue) instrument (NanoTemper Technologies, München, Germany³⁶). With this technique, the diffusion behavior of a labeled protein is measured when an infrared light excites the movement of the protein in capillaries. This behavior is the combination of two effects: the fast, local environment-dependent responses of the fluorophore to the temperature jump and the slower diffusive thermophoresis fluorescence changes. It will be modified when the protein is complexed with increasing amounts of unlabeled partners, leading to titration curves that can be fit for K_d estimation³⁶. In practice, *FhTIM* was labeled with the Monolith His-Tag Labeling Kit RED-tris-NTA (NanoTemper Technologies, München, Germany), as described by the manufacturer. The experiments were performed using 20% and 40% MST power and between 20–80% LED power at 24 °C. The MST traces were recorded using the standard parameters: 5 s MST power off, 30 s MST power on, and 5 s MST power off. The compounds were used at high concentrations (around 5 mM) in the bindings check assay with DMSO at 5% v/v. If the binding check was positive, then the affinity determination was performed with the same experimental settings, with serial 2x dilutions of the compound of interest.

Inhibition of Triosephosphate Isomerase. Expression and purification of proteins: *FhTIM*, RabbitTIM and *HsTIM* were expressed in *Escherichia coli* and purified as described in the literature^{31,37}. After purification, the enzyme, dissolved in 100 mM triethanolamine, 10 mM EDTA and 1 mM dithiothreitol (pH 8), was precipitated with ammonium sulfate (75% saturation) and stored at 4 °C. Before use, extensive dialysis against 100 mM triethanolamine/10 mM EDTA (pH 7.4) was performed. Protein concentration was determined by absorbance at 280 nm for *FhTIM* ($\epsilon = 33,460 \text{ M}^{-1} \text{ cm}^{-1}$) and for RabbitTIM and *HsTIM* ($\epsilon = 33,460 \text{ M}^{-1} \text{ cm}^{-1}$). Enzymatic activity was determined following the conversion of glyceraldehydes-3-phosphate into dihydroxyacetone phosphate in a coupled enzyme assay. The decrease in absorbance at 340 nm was followed in a multiplate reader VarioskanTM Flash Multimode Reader (Thermo ScientificTM, Waltham, MA, USA) at 38 °C. The reaction mixture (1 mL, pH 7.4) contained 100 mM triethanolamine, 10 mM EDTA, 0.2 mM NADH, 1 mM glyceraldehydes-3-phosphate and 0.9 units of α -glycerol phosphate dehydrogenase. The reaction was initiated by the addition of 5 ng/mL of the TIM of interest. For the inhibition studies, TIM was incubated at a concentration of 5 mg/mL in a buffer containing 100 mM triethanolamine, 10 mM EDTA, pH 7.4 and 10% of DMSO at 37 °C for 1 h. The mixture also contained the compounds, dissolved in DMSO, at the indicated concentrations. After 1 h, 10 μ L were withdrawn and added to a final volume of 100 μ L of the reaction mixture for the activity assay. The inhibition assay was performed in a 96-well microplate. None of the molecules tested here affected the activity of α -glycerol phosphate dehydrogenase, the enzyme used in the coupled assay. The IC_{50} value was taken as the concentration of drug needed to reduce the enzymatic activity to 50% by analysis using OriginLab8.5[®] sigmoidal regression (% of enzymatic activity vs. the logarithm of the compound concentration). The experiments were performed in triplicate in two independent experiments.

***FhTIM* crystallization.** *FhTIM* was resuspended at 30 mg/mL in 100 mM triethanolamine/10 mM EDTA (pH 7.4) and stored at -80 °C until use. Protein and crystallization conditions were equilibrated at 19 °C for two hours before preparing the drops. The screening was performed in 96-wells plates using a Mosquito Nanopipetter (TTP Labtech) and commercial screens (Hampton Research, Qiagen) with the sitting drop method, at 19 °C in a Rockimager crystal farm (Formulatrix). Hits grew within 2 weeks in condition B2 of the PEGs II screen (Qiagen). Bigger crystals were grown using the hanging drop method by mixing 1 to 2 μ L of protein solution with an equal amount of crystallization condition (0.1 M MES pH 6.5, 0.01 M ZnSO_4 , 50% PEG550mme). Crystals appeared within two weeks and were directly snap-frozen in liquid nitrogen before being submitted to X-ray diffraction.

X-ray data collection and structure determination. X-ray data were collected at 1.9 Å on beamline ID23-1 from European Synchrotron Radiation Facility, Grenoble, France at 100 K using wavelength $\lambda = 0.97242$ Å. Data were processed in space group $P3_1$ with cell dimensions $a = b = 87.4$ Å $c = 186.6$ Å, $\alpha = \beta = 90^\circ$ and $\gamma = 120^\circ$. Indexation and scaling were performed using XDS and XSCALE programs³⁸. Molecular replacement was performed with the Phaser software³⁹ and using the A chain of Chicken TIM (69% sequence homology, PDB: 4P61)⁴⁰ as a search model with 6 molecules in the asymmetric unit. Initial refinement was performed with Phenix⁴¹ using twin law $-h-k, k, -l$. Water molecules were added during Phenix refinement. After manual curation of the structure (manual placement of the β/α loop 6 (residues 168–180), manual addition of 6 molecules of SO_4 , tidying up water molecules) using WinCoot⁴², further refinements were performed using Refmac 5.8.0238 from the CCP4 suite⁴³. The structure was refined to a final R_{work} of 19.6% and R_{free} of 22.4%, respectively. Statistics of the X-ray data are shown in Table 3. Geometry analysis using Rampage⁴⁴ showed 96% of the residues in preferred regions, 3.6% in allowed regions, and 6 residues (0.4%) as Ramachandran outliers (residues 102 and 156 from chain B, E and F).

Docking. The present crystal structure of *FhTIM* was used as a target in the subsequent docking studies. Compounds were modeled using their SMILES codes from the Chemoffice software. Then, both target protein and ligands were prepared using AutoDockTools v1.5.6⁴⁵: the polar hydrogen atoms were added, the non-polar hydrogens were merged, and the Gasteiger partial atomic charges were calculated. Finally, all the possible rotatable bonds were assigned for each compound. Four distinct docking experiments were then carried out with the program AutoDock Vina v1.1.2⁴⁶: a search on the entire surface of *FhTIM* in its dimeric and monomeric forms as well as a targeted docking in the active site only, with and without flexibility of the side chains of the residues defining the binding pocket. Compounds were treated as fully flexible in each experiment. The search grid was defined accordingly in order to encompass the considered areas. A visual examination of the resulting poses was performed using PyMOL (Schrödinger, Delano Scientific, LLC, New York, NY, USA).

Data collection	<i>Fh</i> TIM	Refinement	<i>Fh</i> TIM
Space group	P3 ₁	Resolution range (Å)	20-1.9
Unit cell parameters			
<i>a</i> , <i>b</i> , <i>c</i> (Å)	87.4, 87.4, 186.6	Number of unique reflections	107970
α , β , γ (°)	90, 90, 120		
Resolution range (Å)	20-1.9 (1.95-1.9)	R _{work} (%)	19.6
R _{sym} (%)	14.4 (152.5)	R _{free} (%)	22.4
I/ σ I	5.11 (0.76)	Number of proteins atoms	11568
Completeness (%)	98.7 (92.9)	Number of water/SO4	1116/6
Redundancy	5.15	Mean B-factor (Å ²)	18.13
Coordinate deviations			
RMSD bond lengths (Å)			0.01
RMSD angles (°)			1.9
PDB ID			6R8H

Table 3. Summary of X-ray data collection and refinement statistics. Values in parentheses are for the highest-resolution shell.

Cell culture. J774.1 murine macrophage cells (ATCC, USA) were grown in DMEM culture milieu containing 4 mM glutamine and supplemented with 10% FCS²⁰. The cells were seeded in a 96-well plate (5×10^4 cells in 200 μ L culture medium) and incubated at 37 °C in a 5% CO₂ atmosphere for 48 h, to allow cell adhesion prior to drug testing. Afterward, cells were exposed for 48 h to the compounds (25–400 μ M) or the vehicle for control (0.4% DMSO), and additional controls (cells in medium) were used in each test. Cell viability was then assessed by measuring the mitochondria-dependent reduction of MTT (3-(4,5-dimethylthiazol-2-yl)-2,5-diphenyltetrazolium bromide) to formazan. For this purpose, MTT in sterile PBS (0.2% glucose), pH 7.4, was added to the macrophages to achieve a final concentration of 0.1 mg/mL, and the cells were incubated at 37 °C for 3 h. After removing the medium, formazan crystals were dissolved in 180 μ L of DMSO and 20 μ L of MTT buffer (0.1 M glycine, 0.1 M NaCl, 0.5 mM EDTA, pH 10.5), and the absorbance at 560 nm was measured. The IC₅₀ was defined as the drug concentration at which 50% of the cells were viable, relative to the control (no drug added), and was determined by analysis using OriginLab8.5[®] sigmoidal regression (% of viable cells vs. the logarithm of the compound concentration). Tests were performed in triplicate.

Cytotoxicity assay on bovine spermatozoa. Semen samples were obtained from a healthy fertile Hereford bull and kept frozen in 0.5 mL straws (extended in Andromed, Minitube, Germany⁴⁷) under liquid nitrogen until use. The semen used belonged to a single freezing batch that was obtained during a regular collection schedule with an artificial vagina. Samples from three straws were thawed and a sperm pool was prepared in PBS at a concentration of 40 million spermatozoa per mL, then 50 μ L of this sperm suspension was carefully mixed with 50 μ L of compounds diluted to 100, 50, 25, 12.5 and 6.25 μ M or with 1% DMSO in control experiments. Each condition was assayed by duplicate in 96-well plates and controls were assayed by triplicate. Plates were incubated at 37 °C for 1 h with moderate shaking. The motility analysis was carried out using a CASA (Computer Assisted Semen Analyzer) system Androvision (Minitube, Tiefenbach, Germany) with an Olympus BX 41 microscope (Olympus, Japan) equipped with a warm-stage at 37 °C. Each sample (10 μ L) was placed onto a Makler Counting Chamber (depth 10 μ m, Sefi-Medical Instruments, Israel) and the following parameters were evaluated: percentage of total motile spermatozoa (motility >5 μ m/s) and velocity curved line (VCL, >24 μ m/s). At least 400 spermatozoa were analyzed from each sample from at least four microscope fields.

In vitro NEJ treatment. *F. hepatica* metacercariae were acquired from DILAVE, MGAP, Uruguay. NEJ were obtained by *in vitro* excystment as previously described with minor modifications⁴⁷. Briefly, metacercariae were incubated with 1% sodium hypochlorite for 5 min at room temperature to remove the outer cyst wall and then washed exhaustively with PBS 200 U/mL Penicillin G sulfate, 200 mg/mL streptomycin sulfate, 500 ng/mL amphotericin B, 10 mM HEPES, counted and divided into groups of around 20 parasites that were transferred to 12 wells tissue culture plates. Parasites were maintained at 37 °C, 5% CO₂ in modified Basch's medium⁴⁷. At day 1, compounds were added at the indicated concentrations and 0.5% DMSO was added to control groups; each condition was tested in duplicate. NEJ behavior was monitored under a light microscope (Olympus BX41), every day each well was recorded for a minute in order to assess parasite motility and registered using the following score: 3- normally active; 2- reduced activity (sporadic movement); 1- immotile (dead)⁴⁸.

Ex-vivo in the adult form of *F. hepatica*. *F. hepatica* were collected from natural infections of cattle obtained from Casablanca slaughterhouse in Paysandú, Uruguay⁴⁹. During slaughter (500 animals observed) the livers that showed signs of fascioliasis (thickened canaliculi) were dissected and adult flukes were recovered and kept in PBS at 37 °C until used (no more than 8 h). After flukes emptied their gut content (i.e. the gut was not dark anymore) they were transferred to 6 well plates (one fluke per well) with 2 mL of RPMI 1640 media with 200 U/mL Penicillin G sulfate, 200 mg/mL streptomycin sulfate, 500 ng/mL amphotericin B and 10 mM glucose at 37 °C. Compounds were added at a concentration of 25 μ M. The antiparasitic efficacy was expressed as the percentage reduction of the number of flukes in the treated group compared with the control group.

***S. mansoni*: treatment of somules *in vitro* and adults *ex vivo*.** The NMRI isolate of *S. mansoni* was maintained by passage through *Biomphalaria glabrata* snails and 3–5 week-old, female Golden Syrian hamsters (Charles River, San Diego, CA) as intermediate and definite hosts, respectively. A dose of 600 infective larvae (cercariae) was used to infect hamsters. The acquisition, preparation and *in vitro* maintenance of *S. mansoni* post-infective larvae (schistosomula or somules) and adults have been already described^{5,50,51}. Vertebrate animal maintenance and handling at the University of California San Diego Animal Care Facility were in accordance with protocols approved by the university's Institutional Animal Care and Use Committee (IACUC).

Phenotypic screens with somules were performed as described^{5,50,51}. Initially, 100 μ L Basch medium⁵², 100 U/ml penicillin, 100 mg/ml streptomycin, 4% heat-inactivated FBS (Corning Mediatech) and 1 μ L compound in DMSO were added to clear, 96-well round-bottomed plates (Costar cat.# 3367). Then, 100 μ L of the same medium containing 40–50 somules was added to mix the compound with somules (final concentration of DMSO was 0.5%). Assay plates were placed into plastic boxes humidified with wet tissue and then incubated at 37 °C in a 5% CO₂ environment. Somules phenotypes were recorded every 24 h up to 72 h using an inverted microscope (Zeiss Axiovert 40C).

Phenotypic screens with 42-day-old, adult parasites were performed in 24-well plates (Costar cat.# 3526) containing the above medium and approximately five adult males and two females per well. Compound was added in a volume of up to 1 μ L DMSO at a concentration of 5 μ M (0.05% DMSO final). Assay plates were incubated at 37 °C in a 5% CO₂ environment. Parasite phenotypes were recorded at 4, 8 and 24 h using a Zeiss Axiovert 40 C.

Schistosome phenotypic responses were recorded employing a series of 'descriptors', such as rounding, degeneration, overactivity, loss of translucency and changes in motility, as described previously^{5,50,51,53}. To allow for comparisons of compound activity, each descriptor was awarded a value of 1 and these were added up to a maximum 'severity score' of 4. Evidence of degeneracy or death was awarded the maximum score of 4. Scores were averaged across duplicate wells for each compound (see details in the supporting information).

Acute oral toxicity. The *in vivo* 50% lethal dose (LD₅₀) was determined according to the guidelines of the Organization for Economic Cooperation and Development (OECD)^{54,55}. All procedures involving animals were approved by the Universidad de la República's Committee on Animal Research (CHEA Protocol ID 707). Briefly, healthy young adult male BALB/c mice (30 days old, 25 to 30 g) were used in this study. Initially, Compound **187** dissolved in vehicle was administered at 2,000 mg/kg, by orogastric cannula, to one animal. The animal was fasted, maintained, and observed for 14 days according to the OECD guidelines. If the mouse survived for the first 48 h, another animal received the same dose. If this was repeated, a third animal was dosed with 2,000 mg/kg and also observed for 14 days. The experiment ends at 14 days post-administration, if there are no signs of toxicity, the (LD₅₀) is the administered dose, if not, the software AOT AOT425 Stat program recommendation was followed. For the vehicle preparation⁵⁶ compound **187** was disposed in a mixture, composed of a surfactant (10%), containing Eumulgin HRE 40 (polyoxyl-40hydrogenated castor oil), sodium oleate, and soya phosphatidylcholine (8:6:3), and an oil phase (10%) containing cholesterol and phosphate buffer (pH 7.4) (80%). Compound **187** was pulverized in a mortar with cholesterol, Eumulgin HRE 40, and phosphatidylcholine, then the mixture was dissolved in chloroform and the solvent was evaporated under vacuum to dryness. In parallel, sodium oleate was dissolved in phosphate buffer and left in an orbital shaker for 12 h at room temperature. The former was then added to the evaporated residue, and the mixture was homogenized and placed in an ultrasonic bath at full power for 30 min. The sample was kept at room temperature until use.

Mouse infection with *F. hepatica*. Six- to eight-week-old female BALB/c mice were obtained from DILAVE Laboratories⁵⁷ (Uruguay). Animals were kept in the animal house (URBE, Facultad de Medicina, UdelaR, Uruguay) with water and food supplied ad libitum. Mouse handling and experiments were carried out in accordance with strict guidelines from the National Committee on Animal Research (CNEA, Uruguay). All procedures involving animals were approved by the Universidad de la República's Committee on Animal Research (CHEA Protocol Number: 070153-000180-16). BALB/c mice were orally infected with 10 *F. hepatica* metacercariae per animal. After 1 week post-infection (wpi), mice were intragastrically inoculated with compound **187** (100 mg/kg) or **TCZ** (100 mg/kg). At 3 wpi mice were bled and sacrificed. Peritoneal exudate cells, spleens, and livers were removed and analyzed. In order to evaluate the severity of the infection, a disease severity score was developed (Table 3S Supporting Information)⁵⁷, which was applied in blinded experiments. Alanine aminotransferase (ALT) activity in sera was determined using a commercial kit (Spinreact, Spain) according to the manufacturers' instructions. PECs from infected and non-infected mice were washed twice with PBS containing 2% FBS and 0.1% sodium azide.

Ethical approval. The study was approved by the Universidad de la República's Committee on Animal Research (CHEA Protocol Number: 070153-000180-16 and ID 707) Review Boards. Under the rules of Comisión Nacional de Experimentación Animal: (CNEA, <http://www.cnea.gub.uy/>).

***In silico* pharmacokinetic parameters.** The predictions were obtained from the online free software SwissADME (<http://www.swissadme.ch>): a free web tool to evaluate pharmacokinetics, drug-likeness and medicinal chemistry friendliness of small molecules⁵⁸. The smiles codes were provided for the software to calculate and the parameters.

Statistical analysis. All statistical tests were performed using Microsoft Excel. Student's t-test (two-tailed distribution) was used to calculate *P* values. The number of experiments and samples was described in the figure legends. All data obtained in more than three experiments or samples show the mean \pm s.d. Nonlinear least-squares fitting was performed using KaleidaGraph Ver. 4.5 to evaluate inhibition activity of compounds (IC₅₀).

Received: 16 September 2019; Accepted: 29 January 2020;

Published online: 13 February 2020

References

1. Renslo, A. R. & McKerrow, J. H. Drug discovery and development for neglected parasitic diseases. *Nat. Chem. Biol.* **2**, 701–710 (2006).
2. Robinson, M. W. & Dalton, J. P. Zoonotic helminth infections with particular emphasis on fasciolosis and other trematodiasis. *Philos. Trans. R. Soc. B Biol. Sci.* **364**, 2763–2776 (2009).
3. Tielens, A. G. M., Van Der Meer, P. & Van Den Bergh, S. G. *Fasciola hepatica*: Simple, large-scale, *in vitro* excystment of metacercariae and subsequent isolation of juvenile liver flukes. *Exp. Parasitol.* **51**, 8–12 (1981).
4. Kelley, J. M. *et al.* Current Threat of Triclabendazole Resistance in *Fasciola hepatica*. *Trends Parasitol.* **32**, 458–469 (2016).
5. Abdulla, M. H. *et al.* Drug discovery for schistosomiasis: Hit and lead compounds identified in a library of known drugs by medium-throughput phenotypic screening. *PLoS Negl. Trop. Dis.* **3**, e478 (2009).
6. Duthaler, U., Smith, T. A. & Keiser, J. *In vivo* and *in vitro* sensitivity of *Fasciola hepatica* to triclabendazole combined with artesunate, artemether, or OZ78. *Antimicrob. Agents Chemother.* **54**, 4596–4604 (2010).
7. Pinto-almeida, A., Mendes, T., Ferreira, P., Belo, S. & De, F. Comparative Proteomics Reveals Characteristic Proteins on Praziquantel-resistance in *Schistosoma mansoni*. *bioRxiv* (2018).
8. Zinsser, V. L., Hoey, E. M., Trudgett, A. & Timson, D. J. Biochemical characterisation of triose phosphate isomerase from the liver fluke *Fasciola hepatica*. *Biochim.* **95**, 2182–9 (2013).
9. Zinsser, V. L., Hoey, E. M., Trudgett, A. & Timson, D. J. Biochemical characterisation of glyceraldehyde 3-phosphate dehydrogenase (GAPDH) from the liver fluke, *Fasciola hepatica*. *Biochim. Biophys. Acta - Proteins Proteom.* **1844**, 744–749 (2014).
10. Dax, C. *et al.* Selective irreversible inhibition of fructose 1,6-bisphosphate aldolase from *Trypanosoma brucei*. *J. Med. Chem.* **49**, 1499–1502 (2006).
11. Mande, S. C. *et al.* Crystal structure of recombinant human triosephosphate isomerase at 2.8 Å resolution. Triosephosphate isomerase-related human genetic disorders and comparison with the trypanosomal enzyme. *Protein Sci.* **3**, 810–821 (1994).
12. Rodríguez-bolaños, M. & Perez-montfort, R. Medical and Veterinary Importance of the Moonlighting Functions of Triosephosphate Isomerase. *Curr. Protein Pept. Sci.* **20**, 304–315 (2019).
13. Rodríguez-Romero, A. *et al.* Structure and inactivation of triosephosphate isomerase from *Entamoeba histolytica*. *J. Mol. Biol.* **322**, 669–675 (2002).
14. Téllez-Valencia, A. *et al.* Inactivation of Triosephosphate Isomerase from *Trypanosoma cruzi* by an Agent that Perturbs its Dimer Interface. *J. Mol. Biol.* **341**, 1355–1365 (2004).
15. Maithal, K., Ravindra, G., Balaram, H. & Balaram, P. Inhibition of *Plasmodium falciparum* triose-phosphate isomerase by chemical modification of an interface cysteine: Electrospray ionization mass spectrometric analysis of differential cysteine reactivities. *J. Biol. Chem.* **277**, 25106–25114 (2002).
16. Téllez-Valencia, A. *et al.* Highly specific inactivation of triosephosphate isomerase from *Trypanosoma cruzi*. *Biochem. Biophys. Res. Commun.* **295**, 958–963 (2002).
17. Alvarez, G. *et al.* Massive screening yields novel and selective *Trypanosoma cruzi* triosephosphate isomerase dimer-interface-irreversible inhibitors with anti-trypanosomal activity. *Eur. J. Med. Chem.* **45**, 5767–5772 (2010).
18. Saramago, L. *et al.* Novel and Selective Rhipicephalus microplus Triosephosphate Isomerase Inhibitors with Acaricidal Activity. *Vet. Sci.* **5**, 74 (2018).
19. Zinzalla, G. & Thurston, D. E. Targeting protein-protein interactions for therapeutic intervention: a challenge for the future. *Future Med. Chem.* **1**, 65–93 (2009).
20. Aguilera, E. *et al.* Potent and Selective Inhibitors of *Trypanosoma cruzi* Triosephosphate Isomerase with Concomitant Inhibition of Cruzipain: Inhibition of Parasite Growth through Multitarget Activity. *Chem. Med. Chem.* **11**, 1328–1338 (2016).
21. Rakus, D., Skalecki, K. & Dzugaj, A. Kinetic properties of pig (*Sus scrofa domestica*) and bovine (*Bos taurus*) D-fructose-1,6-bisphosphate 1-phosphohydrolase (F1,6BPase): Liver-like isozymes in mammalian lung tissue. *Comp. Biochem. Physiol. - B Biochem. Mol. Biol.* **127**, 123–134 (2000).
22. Wei, L. *et al.* Metabolic profiling studies on the toxicological effects of realgar in rats by (1)H NMR spectroscopy. *Toxicol. Appl. Pharmacol.* **234**, 314–25 (2009).
23. Roland, B. P. *et al.* Triosephosphate Isomerase I170V Alters Catalytic Site, Enhances Stability and Induces Pathology in a *Drosophila* Model of TPI Deficiency. *Biochim. Biophys. Acta.* **1852**, 61–69 (2015).
24. Mukherjee, S., Roychowdhury, A., Dutta, D. & Das, A. K. Crystal structures of triosephosphate isomerase from methicillin resistant *Staphylococcus aureus* MRSA252 provide structural insights into novel modes of ligand binding and unique conformations of catalytic loop. *Biochim.* **94**, 2532–2544 (2012).
25. Robinson, M. W., Trudgett, A., Hoey, E. M. & Fairweather, I. Triclabendazole-resistant *Fasciola hepatica*: β -tubulin and response to *in vitro* treatment with triclabendazole. *Parasitology* **124**, 325–338 (2002).
26. Rufener, L., Kaminsky, R. & Mäser, P. *In vitro* selection of *Haemonchus contortus* for benzimidazole resistance reveals a mutation at amino acid 198 of β -tubulin. *Mol. Biochem. Parasitol.* **168**, 120–122 (2009).
27. Ali, I., Lone, M. N. & Aboul-Enein, H. Y. Imidazoles as potential anticancer agents. *Medchemcomm* **8**, 1742–1773 (2017).
28. Fetterer, R. H. The effect of albendazole and triclabendazole on colchicine binding in the liver fluke *Fasciola hepatica*. *J. Vet. Pharmacol. Ther.* **9**, 49–54 (1986).
29. Olivares-Illana, V. *et al.* Perturbation of the dimer interface of triosephosphate isomerase and its effect on *Trypanosoma cruzi*. *PLoS Negl. Trop. Dis.* **1**, e01–08 (2007).
30. McArthur, C., Gallazzi, F., Quinn, T. P. & Singh, K. HIV Capsid Inhibitors Beyond PF74. *Diseases*. **30**, pii: E56 (2019).
31. Minini, L. *et al.* Molecular docking and molecular dynamics simulation studies of *Trypanosoma cruzi* triosephosphate isomerase inhibitors. Insights into the inhibition mechanism and selectivity. *J. Mol. Graph. Model.* **58**, 40–49 (2015).
32. Ross, F. *et al.* Identification of thioredoxin glutathione reductase inhibitors that kill cestode and trematode parasites. *PLoS One* **7**, e35033 (2012).
33. Castro, A. *et al.* Non-ATP competitive glycogen synthase kinase 3beta (GSK-3beta) inhibitors: study of structural requirements for thiazolidinone derivatives. *Bioorg. Med. Chem.* **16**, 495–510 (2008).
34. Alvarez, G. *et al.* New chemotypes as *Trypanosoma cruzi* triosephosphate isomerase inhibitors: a deeper insight into the mechanism of inhibition. *J. Enzyme Inhib. Med. Chem.* **29**, 198–204 (2014).
35. Gerpe, A. *et al.* Indazole N-oxide derivatives as antiprotozoal agents: Synthesis, biological evaluation and mechanism of action studies. *Bioorganic Med. Chem.* **14**, 3467–3480 (2006).
36. Sierra, N. *et al.* Looking for novel capsid protein multimerization inhibitors of feline immunodeficiency virus. *Pharmaceuticals* **11** (2018).
37. Alvarez, G. *et al.* 1,2,4-thiadiazol-5(4H)-ones: a new class of selective inhibitors of *Trypanosoma cruzi* triosephosphate isomerase. Study of the mechanism of inhibition. *J. Enzyme Inhib. Med. Chem.* **5**, 981–989 (2013).
38. Kabsch, W. XDS. *Acta Crystallogr. Sect. D. Biol. Crystallogr.* **D66**, 125–132 (2010).
39. McCoy, A. J. *et al.* Phaser crystallographic software. *J. Appl. Crystallogr.* **40**, 658–674 (2007).
40. Zhai, X. *et al.* Enzyme Architecture: The Effect of Replacement and Deletion Mutations of Loop 6 on Catalysis by Triosephosphate Isomerase. *Biochem.* **53**, 3486–3501 (2014).
41. Adamsa, P. D. *et al.* The Phenix Software for Automated Determination of Macromolecular Structures. *Methods* **55**, 94–106 (2012).
42. Emsley, P., Lohkamp, B., Scott, W. G. & Cowtan, K. Features and development of Coot. *Acta Crystallogr. Sect. D. Biol. Crystallogr.* **66**, 486–501 (2010).

43. Winn, M. D. *et al.* Overview of the CCP 4 suite and current developments. *Acta Crystallogr. Sect. D. Biol. Crystallogr.* **D67**, 235–242 (2011).
44. Lovell, S. C. *et al.* Structure Validation by C Geometry: and C Deviation. *PROTEINS Struct. Funct. Genet.* **50**, 437–450 (2003).
45. Morris, G. M. *et al.* AutoDock4 and AutoDockTools4: Automated docking with selective receptor flexibility. *J. Comput. Chem.* **30**, 2785–2791 (2009).
46. Trott, O. & Olson, A. J. AutoDock Vina: improving the speed and accuracy of docking with a new scoring function, efficient optimization, and multithreading. *J. Comput. Chem.* **31**, 455–461 (2010).
47. Ferraro, F. *et al.* Identification of Chalcones as Fasciola hepatica Cathepsin L Inhibitors Using a Comprehensive Experimental and Computational Approach. *PLoS Negl. Trop. Dis.* **10**, e0004834 (2016).
48. Ferraro, F. *et al.* Cathepsin L Inhibitors with Activity against the Liver Fluke Identified from a Focus Library of Quinoxaline1,4-di-N-Oxide Derivatives. *Molecules.* **24**, 2348 (2019).
49. Bennett, J. L. & Keehler, P. Fasciola hepatica: Action *in vitro* of triclabendazole on immature and adult stages. *Exp. Parasitol.* **63**, 49–57 (1987).
50. Long, T. *et al.* Phenotypic, chemical and functional characterization of cyclic nucleotide phosphodiesterase 4 (PDE4) as a potential anthelmintic drug target. *PLoS Negl. Trop. Dis.* **11**, e0005680 (2017).
51. Long, T. *et al.* Structure-Bioactivity Relationship for Benzimidazole Thiophene Inhibitors of Polo-Like Kinase 1 (PLK1), a Potential Drug Target in Schistosoma mansoni. *Plos Negl. Trop. Dis.* **10**, e0004356 (2016).
52. Basch, P. F. Cultivation of *Schistosoma mansoni* *In vitro*. I. Establishment of Cultures from Cercariae and Development until Pairing. *J. Parasitol.* **67**, 179–185 (1981).
53. Kyere-Davies, G. *et al.* Effect of Phenotypic Screening of Extracts and Fractions of Erythrophleum ivorense Leaf and Stem Bark on Immature and Adult Stages of Schistosoma mansoni. *J. Parasitol. Res.* ID **9431467** (2018).
54. OECD Guidelines for the Testing of Chemicals, Section 4, Test No. 425: Acute Oral Toxicity - Up-and-Down Procedure. *Guidel. Test. Chem.* **26** (2001).
55. Alvarez, G. Bioguided Design of Trypanosomicidal Compounds: in *Methods and Protocols. Methods Mol. Biol.* **1824**, 139–163 (2018).
56. Álvarez, G. *et al.* Identification of a new amide-containing thiazole as a drug candidate for treatment of chagas' disease. *Antimicrob. Agents Chemother.* **59**, 1398–1404 (2015).
57. Carasi, P. *et al.* Heme-oxygenase-1 expression contributes to the immunoregulation induced by Fasciola hepatica and promotes infection. *Front. Immunol.* **8**, 1–15 (2017).
58. Daina, A., Michielin, O. & Zoete, V. SwissADME: A free web tool to evaluate pharmacokinetics, drug-likeness and medicinal chemistry friendliness of small molecules. *Sci. Rep.* **7**, 1–13 (2017).

Acknowledgements

We thank UK embassy in Uruguay for the supporting grant Science and Innovation Fund UK_ID_2015_1_6 and PROGRAMA ECOS (U14S01) Proyectos conjuntos de investigación científica Uruguay – Francia. We thank the staff of the Protein Science Facility (PSF) of the UMS BioSciences Gerland-Lyon Sud for assistance with the crystallogeneses experiments. We thank the staff of ID23-1 beamline at the European Synchrotron Radiation Facility (Grenoble, France), and Pr. P. Gouet for his help with the analysis of the diffraction data. Phenotypic screens of *S. mansoni* at the CDIPD (BMS and CRC) were made possible in part by the grant awards R21AI126296 from the NIH and OPP1171488 from the Bill and Melinda Gates Foundation. Dedicated to S.O.A.

Author contributions

G.A., designed and executed chemical, biochemical and cellular experiments and analyzed data. C.G. helped with the M.S.T. and performed the crystallogeneses experiments and structure determination of *FhTIM*. X.R. performed docking experiments and analysis. T.F., performed the *in vivo* animal studies. G.A., C.G., I.C., D.J.T., X.R., C.R.C. wrote the manuscript. A.I. and I.C. optimized the production of *FhTIM*. F.F. and G.A. performed the T.I.M. inhibition screening. F.F., I.C., G.A. and M.C. evaluated the inhibitors against N.E.J. and adult forms of *F. hepatica*. I.C., B.M.S. and C.C. evaluated the inhibitors against *S. mansoni*. L.B. synthesized compounds. F.F. and J.G. performed the sperm toxicity assays. All authors reviewed the manuscript.

Competing interests

The authors declare no competing interests.

Additional information

Supplementary information is available for this paper at <https://doi.org/10.1038/s41598-020-59460-y>.

Correspondence and requests for materials should be addressed to G.Á.

Reprints and permissions information is available at www.nature.com/reprints.

Publisher's note Springer Nature remains neutral with regard to jurisdictional claims in published maps and institutional affiliations.



Open Access This article is licensed under a Creative Commons Attribution 4.0 International License, which permits use, sharing, adaptation, distribution and reproduction in any medium or format, as long as you give appropriate credit to the original author(s) and the source, provide a link to the Creative Commons license, and indicate if changes were made. The images or other third party material in this article are included in the article's Creative Commons license, unless indicated otherwise in a credit line to the material. If material is not included in the article's Creative Commons license and your intended use is not permitted by statutory regulation or exceeds the permitted use, you will need to obtain permission directly from the copyright holder. To view a copy of this license, visit <http://creativecommons.org/licenses/by/4.0/>.

© The Author(s) 2020